Laser Physics Letters

Astro Ltd.

LETTER

Optical clearing of laser-induced tissue plasma

To cite this article: Zhimei Wei *et al* 2021 *Laser Phys. Lett.* **18** 085603

IOP Publishing | Astro Ltd Laser Physics Letters
Laser Phys. Lett. **18** (2021) 085603 (7pp) https://doi.org/10.1088/1612-202X/ac0e40

Letter

Optical clearing of laser-induced tissue plasma

Zhimei Wei[1], Qingyu Lin[2,*], Ekaterina N Lazareva[3,5], Polina A Dyachenko(Timoshina)[3,5], Jie Yang[1], Yixiang Duan[2] and Valery V Tuchin[3,4,5,*]

[1] Institute of Materials Science and Technology, Analytical & Testing Center, Sichuan University, Chengdu 610065, People's Republic of China
[2] Research Center of Analytical Instrumentation, School of Mechanical Engineering, Sichuan University, Chengdu 610065, People's Republic of China
[3] Research-Educational Institute of Optics and Biophotonics, Saratov State University, Saratov 410012, Russia
[4] Laboratory of Laser Diagnostics of Technical and Living Systems, Institute of Precision Mechanics and Control of the RAS, Saratov 410028, Russia
[5] Interdisciplinary Laboratory of Biophotonics, National Research Tomsk State University, Tomsk 634050, Russia

E-mail: qylin@scu.edu.cn and tuchinvv@mail.ru

Received 8 June 2021
Accepted for publication 21 June 2021
Published 6 July 2021

Abstract

We studied the effect of optical clearing (OC) by glycerol on laser-induced tissue plasma using the immersion method. The results demonstrated the apparently enhanced effect of glycerol on the molecular spectra of the laser induced plasma. The OC is more sensitive to the molecular bands than atomic lines. After tissue immersion in the glycerol, the electron density of tissue plasma is decreased. The laser plasma temperature of the glycerol treated tissue is higher than for virgin fresh tissue. The tissue plasma after the glycerol application is still in the local thermal equilibrium plasma state. This work presents a new perspective for OC application that can extend from tissue better imaging quality to improvement of laser plasma generation.

Keywords: laser-induced breakdown spectroscopy, optical clearing, plasma, tissue

(Some figures may appear in colour only in the online journal)

1. Introduction

The optical clearing (OC) technique has been intensively studied for controlling tissue optical properties and effectively reduction light scattering in tissues. Generally, this technique can increase the light penetration depth and reduce the distortion of laser beams with the use of hyperosmotic optical clearing agents (OCAs). Currently, the OCAs with high refractive indices and hyperosmolarity are frequently used to improve the sensitivity in areas of tissue imaging and spectroscopy [1].

The application of OCA on a tissue allows for controlling the optical properties of tissue. OC enables to suppress the scattering of light and allows penetrate more deeply via the application of special OCAs into tissues. At present, OC technique is common in conjunction with Raman spectroscopy [2], optical coherence tomography technique [3], laser speckle imaging [4], photoacoustic flow cytometry [5], multiphoton microscopy [6], and NIR spectroscopy [7]. OC technique has a great potential for spectroscopic investigations in life science owing to its simplicity, low cost, and low risk [8]. The

* Authors to whom any correspondence should be addressed.

laser-induced breakdown spectroscopy (LIBS) technique can be used as a quick analytical tool for tissue. LIBS analysis of paraffin-tissue samples [9, 10], and fresh soft tissue [11] were performed to identify the spectral differences based on different pretreatment methods. LIBS technique provides advantages including simplicity, fast response, and simultaneous multi-elemental analysis. Nowadays, it has been demonstrated that LIBS could be used for the discrimination of tissues suffering minor clinical changes, even may advance the diagnosis of cancer.

In the present work, we focused on the OC combined with the LIBS technique towards tissue analysis to evaluate the effect of OC to the laser plasma. No investigations on evaluating the effect of OC on the laser-induced tissue plasma that have been reported. The plasma temperature and electron density are two important parameters for understanding the plasma processes. Thus, the effect of OCA on the plasma parameters was investigated systematically. To our knowledge, no prior study has addressed this topic.

2. Experiment

The experimental setup details have been previously described elsewhere [9], and therefore only the main components are described in this section. Briefly, a Nd:YAG laser (Lotis, Russia) was used as the excitation source in the experiment. The laser was operated at the fundamental wavelength of 1064 nm, and at the repetition rate of 10 Hz with a pulse duration of 10 ns. The laser beam was perpendicularly focused onto the surface of tissue by a micro-objective lens with a work distance of 15 mm, and the distance was monitored by using two laser-diode pointers in oblique incidence on the sample surface. A motorized XYZ sample stage was used to place the sample. The plasma emission lights were coupled to the optical fiber by utilizing a collimating lens at an accident angle of 45° to the target surface, and then delivered into an echelle spectrometer (LTB-Aryelle200, Germany) equipped with an ICCD camera (Andor, UK). The wavelength calibration of the spectrometer and spectral response of the detection system was performed with its mercury argon lamp and a certified deuterium halogen tungsten light source prior to the experiment, respectively. A laser pulse energy of 100 mJ was used in this work. The focused spot size on the sample surface was estimated to be about 200 μm in diameter, resulting in an estimated laser irradiance of about 30 GW·cm^{-2}, respectively. To perform the statistical analysis, each spectrum were obtained by averaging the signals of 100 ablation events on different sites.

The raw pork tissue samples were purchased from the local markets. Samples collected include liver, fat and muscle. The samples were cut into pieces with approximately 10 mm thickness and stored at 4° until before analysis. The slices of roughly 20 × 20 × 10 mm were further cut before LIBS analysis. Eleven different samples were obtained for each type of tissue, therefore, 33 samples in total were analyzed in this work. The glycerol (Kelong Cto., China) was chosen as an OCA to investigate the OC effect. A concentration of glycerol (99.9%) was topically applied in this wok. The tissue samples were completely immersed with the glycerol. LIBS measurements were performed at time intervals of 24 h following topical application of the glycerol.

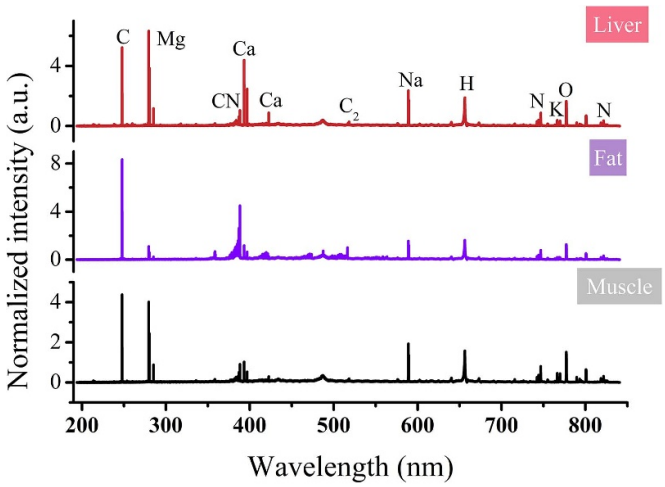

Figure 1. The normalized intensity of spectral lines for tissue samples. All spectra are obtained on soft tissues at room temperature.

3. Results and discussion

3.1. Laser-induced tissue spectroscopy

Figure 1 is the normalized LIBS spectra of liver, fat and muscle tissues. It can be seen that the three types of tissues have similar LIBS spectral profiles. The prominent characteristic emissions of C (247.86 nm), H (656.28 nm), O (777.20 nm), N (744.24 nm, 746.83 nm, 821.68 nm), Mg (279.55 nm, 279.80 nm, 280.27 nm, 285.16 nm), Ca (393.35 nm, 396.84 nm, 422.67 nm), Na (588.97 nm, 589.58 nm), and K (766.45 nm) are identified. These elements within the tissues are assessed by LIBS. The laser will heat the sample in the vicinity of the laser shot, so the water evaporates from the tissue surface. However, it should be noticed that the soft tissue cannot be ablated easily with the IR laser [12]. Moreover, these three types of tissue are characterized with strong molecular emissions of CN (385.44 nm, 386.19 nm, 387.14 nm, 388.34 nm) bands and C_2 (516.48 nm, 512.89 nm) bands. The C_2 and CN bands delineate the cellular ablated fragments. The CN and C_2 emissions of the liver and muscle tissues are much weaker than those of the fat tissue.

Figures 2–5 show the effect of glycerol application on the intensity of the Ca, Mg, Na, and CN spectra, respectively. The enhancement of atomic spectral emission on different elements was not observed. While, the intensity of all the targeted peaks decreased after the treatment with glycerol. Although the glycerol increased the path length of light propagating through the tissue, the results suggested that the sample mass of laser ablation did not increased apparently. Instead due to better focusing the sample mass can be decreased as locality of probing can be increased. Notably, different from the atomic lines, the CN molecular bands show an apparent increased after glycerol application. The 388.34 nm band emitted from

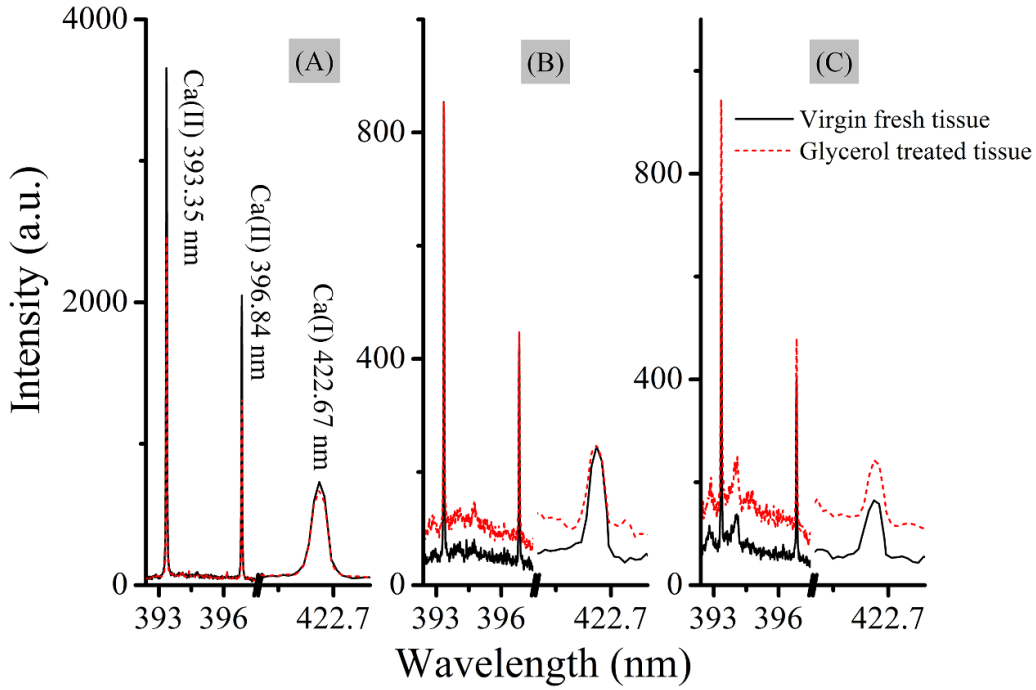

Figure 2. Spectra of Ca II (393.35 nm), Ca II (396.84 nm) and Ca I (422.67 nm) spectral lines for virgin and glycerol treated samples (A) liver (B) muscle (C) fat.

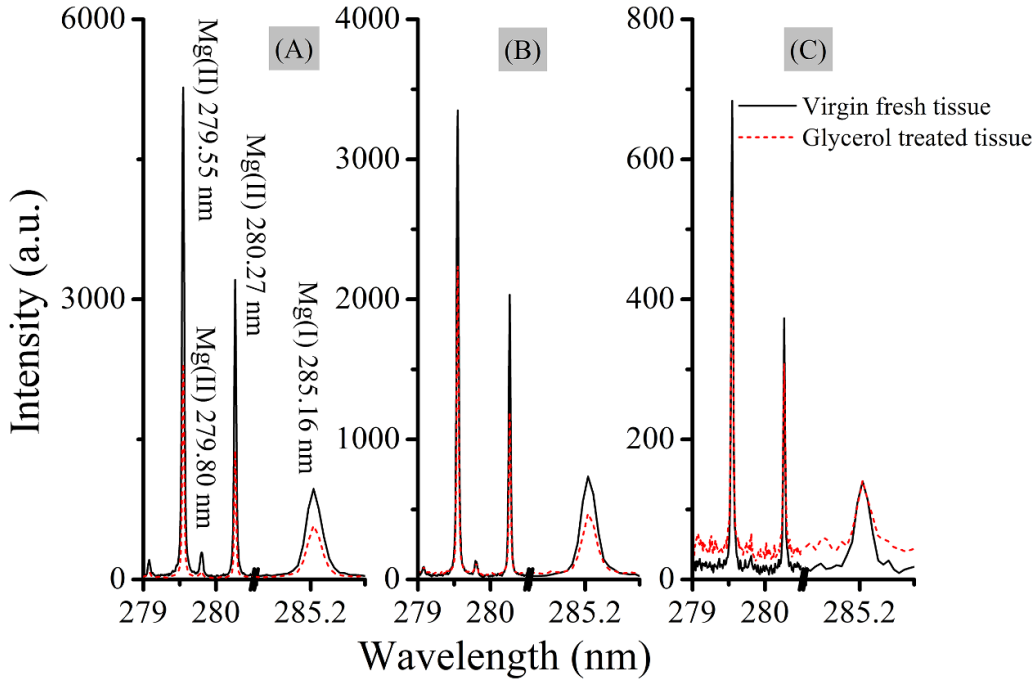

Figure 3. Spectra of Mg II (279.55 nm, 279.80 nm and 280.27 nm) and Mg I (285.16 nm) spectral lines for virgin and glycerol treated samples (A) liver (B) muscle (C) fat.

the muscle tissue experienced about four times enhancement, which is stronger than that of the fat one (about three times) and liver tissue (about two times). These differences in the molecular spectral profiles suggest that the OC is more sensitive to the molecular bands than atomic lines. It may be attributed to the assistant dissociation of organic matter into the tissue.

During the laser ablation of tissue samples, carbon atoms, ions or molecules are ejected from the target and react with N_2 in the ambient air to form CN excited particle emission. Lu *et al* reported that the formation mechanism of CN radical radiation [13]. The CN free radical density is directly related with the rotational temperature and vibration temperature. It mainly occurs in the periphery of plasma close to

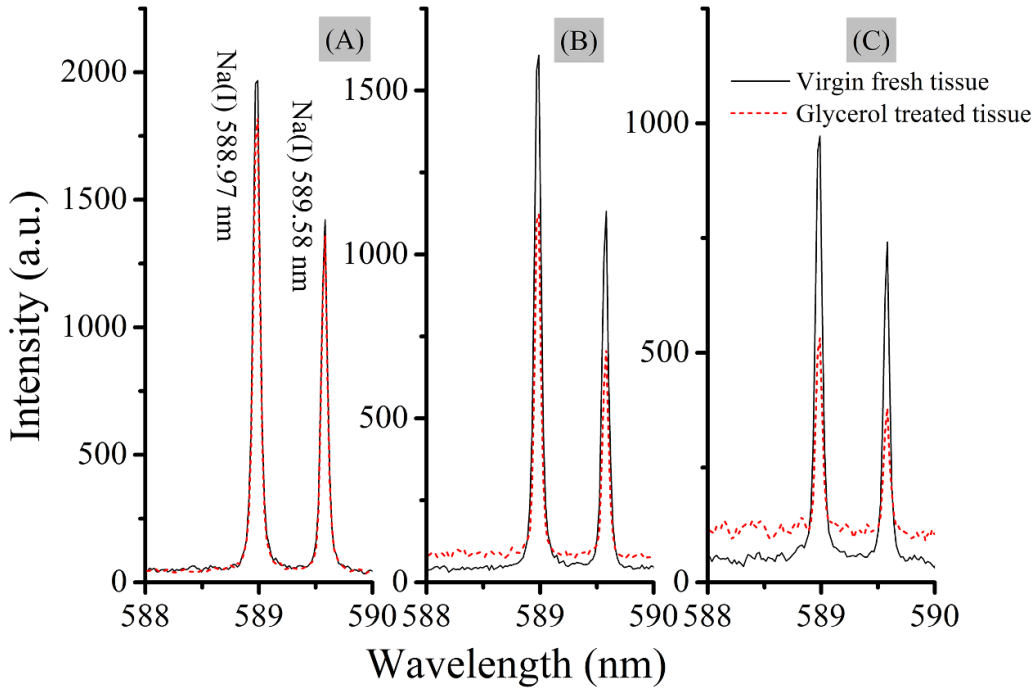

Figure 4. Spectra of Na I (588.97 nm, 589.58 nm) spectral lines for virgin and glycerol treated samples (A) liver (B) muscle (C) fat.

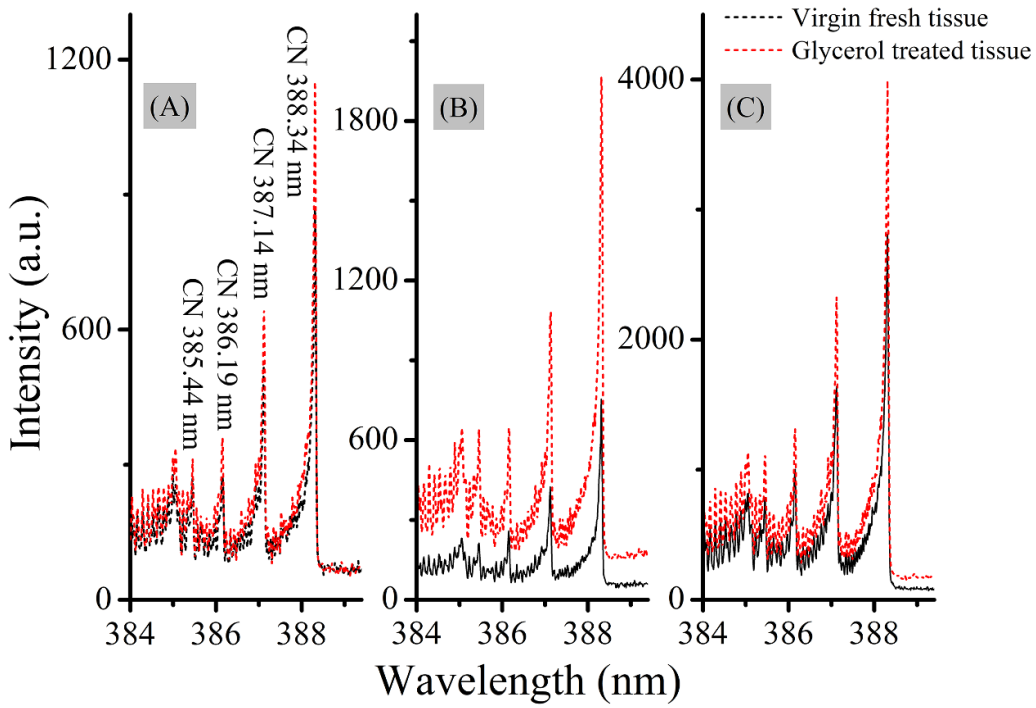

Figure 5. Spectra of CN (385.44 nm, 386.19 nm, 387.14 nm and 388.34 nm) spectral bands for virgin and glycerol treated samples (A) liver (B) muscle (C) fat.

the air. These results demonstrated the apparently enhanced effect of glycerol on the molecular bands of the laser induced plasma. After being immersed with glycerol, the tissue dehydration was induced by the osmotic properties of glycerol [14]. According to Fick's second law of diffusion, due to tissue dehydration, the agent concentration decreases for glycerol and increases for water linearly from the surface to deeper sites of the tissue [15]. Thus, the rapid dehydration further improved the signal of deeper layers, such as collagen and lipid bands in tissue. The assistant dissociation of organic matter will be happened, leading to more generation of C excited species. Therefore, the reaction between C_2^* and N_2 was more promoted in the laser tissue plasma after immersed with glycerol, showing as the increased intensity of CN bands. The

results open a new perspective on the different effects of glycerol in the atomic and molecular spectra in the laser-induced plasma.

3.2. Electron density

Electron density describes the number of free electrons per unit volume. The electron density is determined from the linear Stark broadening of spectral lines. It is based on the assumption that the Stark effect is the dominant peak broadening mechanism, while Doppler broadening and natural broadening can be ignored [16]. The Stark line broadening which is due to the collision between charged species and can be fitted with a Lorentzian distributions [17, 18]. We chose the Mg (I) line at 285.21 nm to evaluate the electron density in this work.

The plasma electron density (N_e) can be calculated by equation (1):

$$N_e = \frac{\Delta\lambda_{st} \times 10^{16}}{2\omega}, \tag{1}$$

where $\Delta\lambda_{st}$ is the full width at half maximum of Stark broadening lines, which is a sensitive function of the Stark broadening mechanism [19]. ω is the electron impact width parameter.

It should be also noticed when calculating the Stark broadening line width, the influence of the instrumental broadening ($\Delta\lambda_{spe}$) should be considered. In this work, the instrumental broadening width was obtained by fitting Hg lines emitted from a certified low-pressure mercury light source and found to be 38.53 pm at 365.48 nm. Thus, the Lorentz fitted spectral line shape was further corrected by subtracting the broadening contribution from the spectrometer (calculated by equation (2))

$$\Delta\lambda = \sqrt{\Delta\lambda_{st}^2 - \Delta\lambda_{spe}^2}. \tag{2}$$

Figure 6 shows that the electron density of laser-plasma from the three types of tissue, respectively. Before being treated with glycerol, the plasma of fresh liver tissue shows the highest electron density, while the plasma of fat tissue shows the lowest value. The reason is mainly the different components of the tissue. It is well known that the fat tissue is composed of three fatty acids and glycerol and exhibits a soft lipid. After immersion with the glycerol, the electron density of the three tissue decreased. The electron density quickly decreased for the fat tissue after treated with glycerol. In laser-induced plasmas, the interactions of radiators and neighboring particles, collisions of ions or extent electrons, are involved by the Stark effect. Therefore, the decrease of the electron density could be attributed to the decline of the collision particles in the laser-induced tissue plasma due to the glycerol application.

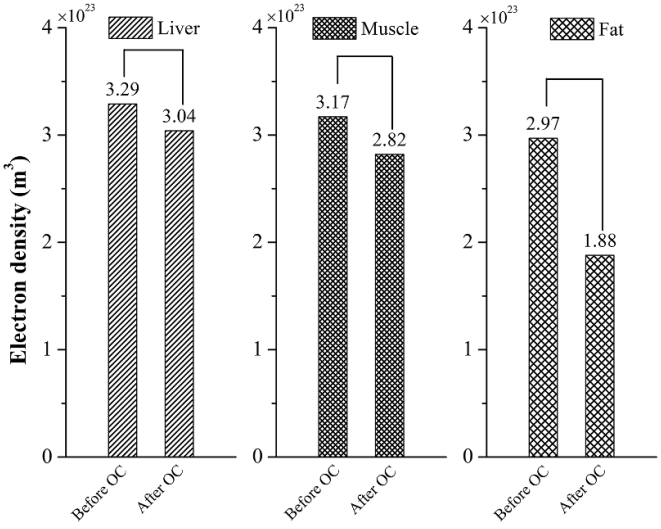

Figure 6. Electron density of LIBS plasma from different tissue.

3.3. Plasma temperatures

The Saha–Boltzmann plot method was used to measure the plasma temperatures. This method is popularly used to calculate plasma temperatures. For the theory of the Saha–Boltzmann method, it is supposed that the species of the different ionization degrees of a given element are in thermodynamic equilibrium with the same temperature. The Saha equation provides relationship between transition line intensities from different ionization stages, while the Boltzmann equation provides relationships between transition line intensities from the same ionization degree [20]. The intensity ratio between the singly ionized and neutral species of the same element can be calculated by equation (3):

$$\frac{I_1}{I_2} = \frac{g_1 A_1 \lambda_2}{g_2 A_2 \lambda_1} \times \frac{2(2\pi m_e \kappa)^{3/2}}{h^3} \frac{1}{n_e} T^{3/2} \times \exp\left(-\frac{E_1 - E_2 + E_{IP} - \Delta E}{\kappa T}\right), \tag{3}$$

where the subscripts 1 and 2 refer to the higher and lower stages of ionization, respectively, n_e is the electron density (cm^{-3}), E_1 and E_2 is the ionization energy (eV), m_e is the mass of the electron (g), h is Planck constant (eV•s), E_{IP} is the ionization potential of the less ionized stage, ΔE is a correction to the ionization potential for interactions in the plasma.

Equation (3) further to be changed to the next and equation (4):

$$\frac{I_1 \lambda_1}{g_1 A_1} = \frac{I_2 \lambda_2}{g_2 A_2} \times \frac{2(2\pi m_e \kappa)^{3/2}}{h^3} \frac{1}{n_e} T^{3/2} \times \exp\left(-\frac{E_1 - E_2 + E_{IP} - \Delta E}{\kappa T}\right). \tag{4}$$

Then, by taking the logarithm of both sides of equation (4), we obtain and equation (5):

Table 1. Spectral parameters of Ca lines.

Line	λ (nm)	A_{ki} (s^{-1})	E_1 (eV)	E_2 (eV)	g_1	g_2	Transition
Ca(II)	393.37	1.47×10^8	0	3.15	2	4	$3p^64s(^2s_{1/2})$ $-3p^64p(^2p_{3/2})$
Ca(II)	396.85	1.40×10^8	0	3.12	2	2	$3p^64s(^2s_{1/2})$ $-3p^64p(^2p_{1/2})$
Ca(I)	422.67	2.18×10^8	0	2.93	1	3	$3p^64s(^1s)$ $-3p^64s4p(^2p_1)$

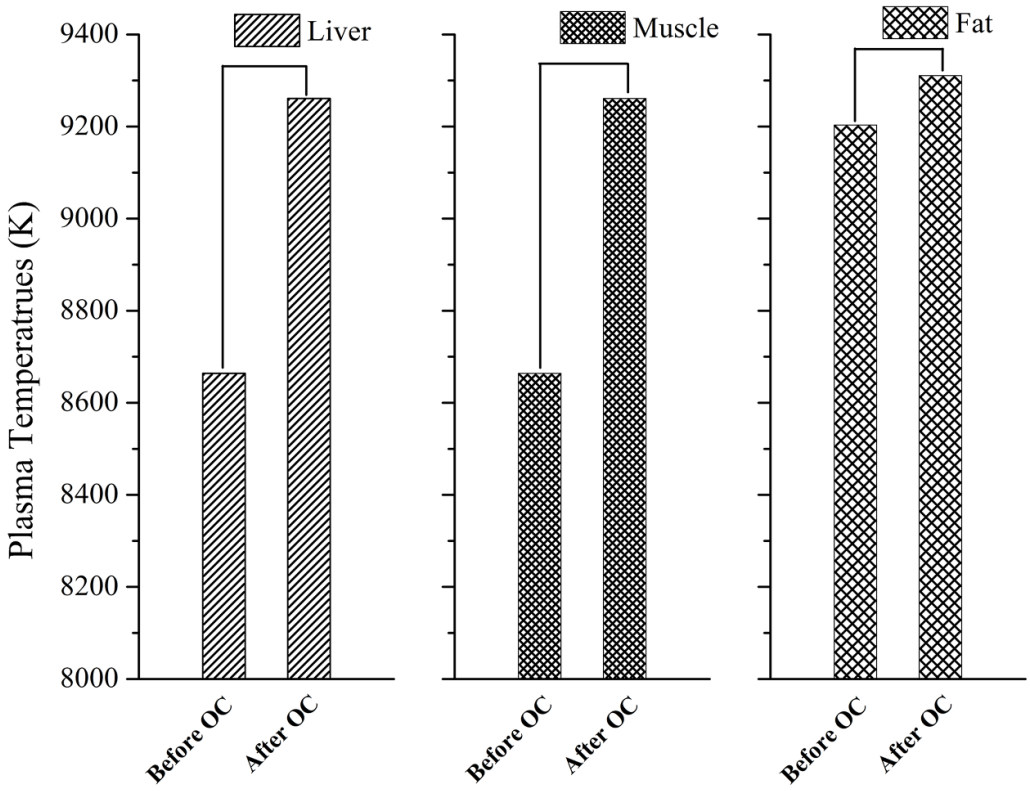

Figure 7. Plasma temperatures of LIBS plasma from different tissue.

$$\ln\left(\frac{I_1\lambda_1}{g_1\,A_1}\right)-\ln\left(\frac{I_2\lambda_2}{g_2\,A_2}\right)=\ln\left(\frac{2(2\pi\,m_e\kappa)^{3/2}}{h^3}\frac{1}{n_e}\,T^{3/2}\right)-\frac{E_1-\,E_2+\,E_{IP}-\Delta E}{\kappa T}. \quad (5)$$

To place neutrals and ions on the same plot, the abscissas and ordinates of the ion point further to be adjusted. The abscissa values of the ion energy levels were modified, defined as $E_1{}^*$. The revised equations list as equations (6)–(8):

$$E_1^*=\,E_1+\,E_{IP}-\Delta E, \quad (6)$$

$$\ln\left(\frac{I_1\lambda_1}{g_1\,A_1}\right)^*=\ln\left(\frac{I_1\lambda_1}{g_1A_1}\right)-\ln\left(\frac{2(2\pi m_e\kappa)^{3/2}}{h^3}\frac{1}{n_e}T^{3/2}\right), \quad (7)$$

$$\ln\left(\frac{I_1\lambda_1}{g_1\,A_1}\right)^*-\ln\left(\frac{I_2\lambda_2}{g_2\,A_2}\right)=-\frac{1}{\kappa_B T}(\,E_1^*-\,E_2). \quad (8)$$

Therefore, the Saha–Boltzmann plot straight line is then achieved with the revised equation, and the slope of the plot is related to the plasma temperature as well. The good linearity of each tissue implies that the electrons are in equilibrium with the neutral atoms. In the present work, the neutral lines and ionic lines of Ca 393.37 nm, 396.85 nm, and 422.67 nm were used to calculate the due to well isolated without overlapping interference by other transitions and measured without self-absorption. The spectral parameters of the three lines are listed in table 1, they can be found from the atomic spectra database in the National Institute of Standards and Technology.

The measured temperatures at different tissues are shown in figure 7. The laser-plasma temperature of the glycerol-treated tissue is higher than the virgin fresh one. The plasma temperature of the liver and muscle represents an increase after glycerol

application. But, the temperature of fat plasma has merely a slight variation with the glycerol immersion. The results suggest that the OCA has ability to increase the plasma temperatures. According to the local thermal equilibrium (LTE) condition, the electron density should be high enough to ensure a high collision rate to dominate the radiative processes. The McWhirter criterion provides the lower limit for the electron number density at which the plasma will be in LTE [21]:

$$N_e \geq 1.6 \times 10^{12} T_e^{1/2} \Delta E^3, \tag{9}$$

where ΔE is the largest energy transition for which the condition holds and T_e is the plasma temperature.

The maximum energy level difference is 3.15 eV, the threshold value of the electron number density is about 4.64×10^{15} cm^{-3} according to formula (9), which is far less than the calculated values of electron number density in the present work. Therefore, in this experiment, the plasma after the glycerol application is also in LTE state.

4. Conclusions

In this study, the responses of laser-induced tissue plasma to OCA were studied using the immersion method. It is a new perspective for OC application. We first demonstrate that the OC can also affect the parameters of laser-induced tissue plasma. It is a prospective application of OC combined with LIBS as an in situ tool for tissue analysis during surgery.

Acknowledgments

The authors are grateful for financial support from the Natural Science Foundation of China (61605134), Sichuan Applied Basic Research Project (2019YJ0078). E N L, P A D, and V V T were supported by a grant under the Decree of the Government of the Russian Federation No. 220 of 9 April 2010 (Agreement No. 075-15-2021-615 of 4 June 2021).

References

[1] Tuchin V V 2005 Optical clearing of tissues and blood using the immersion method *J. Phys. D: Appl. Phys.* **38** 2497–518
[2] Schulmerich M V, Cole J H, Dooley K A, Morris M D, Kreider J M and Goldstein S A 2008 Optical clearing in transcutaneous Raman spectroscopy of murine cortical bone tissue *J. Biomed. Opt.* **13** 021108
[3] Larin K V, Ghosn M G, Bashkatov A N, Genina E A, Trunina N A and Tuchin V V 2012 Optical clearing for OCT image enhancement and in-depth monitoring of molecular diffusion *IEEE J. Sel. Top. Quantum Electron.* **18** 1244–59
[4] Wang J, Zhang Y, Xu T H, Luo Q M and Zhu D 2012 An innovative transparent cranial window based on skull optical clearing *Laser Phys. Lett.* **9** 469–73
[5] Menyaev Y A, Nedosekin D A, Sarimollaoglu M, Juratli M A, Galanzha E I, Tuchin V V and Zharov V P 2013 Optical clearing in photoacoustic flow cytometry *Biomed. Opt. Exp.* **4** 3030–41
[6] Yeh A T, Choi B, Nelson J S and Tromberg B J 2003 Reversible dissociation of collagen in tissues *J. Invest. Dermatol.* **121** 1332–5
[7] Genina E A, Bashkatov A N and Tuchin V V 2017 Optical clearing of human dura mater by glucose solutions *J. Biomed. Photon. Eng.* **3** 010309
[8] Sdobnov A Y, Darvin M E, Genina E A, Bashkatov A N, Lademann J and Tuchin V V 2018 Recent progress in tissue optical clearing for spectroscopic application *Spectrochim. Acta* A **197** 216–29
[9] Lin Q, Wei H, Yin P, Duan Y and Bian F 2020 Discrimination of elemental responsiveness to tumor chemotherapy by laser-induced breakdown spectroscopy coupled with chemometric methods *Laser Phys.* **30** 105701
[10] Teng G, Wang Q, Zhang H, Xiangli W, Yang H, Qi X, Cui X, Idrees B S, Wei K and Khan M N 2020 Discrimination of infiltrative glioma boundary based on laser-induced breakdown spectroscopy *Spectrochim. Acta* B **165** 105787
[11] Li X, Yang S, Fan R, Yu X and Chen D 2018 Discrimination of soft tissues using laser-induced breakdown spectroscopy in combination with k nearest neighbors (kNN) and support vector machine (SVM) classifiers *Opt. Laser Technol.* **102** 233–9
[12] Feldmann J, Kindness A and Ek P 2002 Laser ablation of soft tissue using a cryogenically cooled ablation cell *J. Anal. At. Spectrom.* **17** 813–8
[13] Lu X, Liu Y, Zhang Q and Li L 2020 Study on tea harvested in different seasons based on laser-induced breakdown spectroscopy *Laser Phys. Lett.* **17** 015701
[14] Lin Q, Lazareva E N, Kochubey V I, Duan Y and Tuchin V V 2020 Kinetics of optical clearing of human skin studied in vivo using portable Raman spectroscopy *Laser Phys. Lett.* **17** 105601
[15] Tuchin V V 2008 *Handbook of Optical Sensing of Glucose in Biological Fluids and Tissues* (Boca Raton, FL: CRC Press)
[16] Li Q, Chen A, Zhang D, Wang Q, Xu W, Qi Y, Li S, Jiang Y and Jin M 2021 Time-resolved electron temperature and density of spark discharge assisted femtosecond laser-induced breakdown spectroscopy *Optik* **225** 165812
[17] Bye C A and Scheeline A 1995 Electron density profiles in single spark discharges *J. Quant. Spectrosc. Radiat. Transfer* **53** 75–93
[18] Hermann J, Boulmer-Leborgne C and Hong D 1998 Diagnostics of the early phase of an ultraviolet laser induced plasma by spectral line analysis considering self-absorption *J. Appl. Phys.* **83** 691–6
[19] Sabsabi M and Cielo P 1995 Quantitative analysis of aluminum alloys by laser-induced breakdown spectroscopy and plasma characterization *Appl. Spectrosc.* **49** 499–507
[20] Yalçin S, Crosley D, Smith G and Faris G W 1999 Influence of ambient conditions on the laser air spark *Appl. Phys.* B **68** 121–30
[21] McWhirter R W P 1965 *Plasma Diagnostic Techniques* (New York: Academic)